

## Article

# Mineralization of Octacalcium Phosphate under Magnetic Field

Wenhao He <sup>1,2</sup>, Bingyu Xue <sup>1,2</sup>, Qi Qian <sup>1,2</sup>, Shenye Chen <sup>1,2</sup>, Zhengyi Fu <sup>1,3</sup> and Kun Wang <sup>1,2,\*</sup> <sup>1</sup> Hubei Longzhong Laboratory, Xiangyang 441000, China<sup>2</sup> School of Materials Science and Engineering, Wuhan University of Technology, Wuhan 430070, China<sup>3</sup> State Key Laboratory of Advanced Technology for Materials Synthesis and Processing, Wuhan University of Technology, Wuhan 430070, China

\* Correspondence: kun.wang@whut.edu.cn

**Abstract:** The mineralization of octacalcium phosphate (OCP) crystals in gel media was studied in the presence of a magnetic field. OCP crystal growth was found to be dependent on mineralization temperature, mineralization time, and the magnetic field. Higher temperatures significantly reduced the mineralization time, which is crucial for directional growth of OCP crystals. The growth of OCP crystals was accelerated by the applied magnetic field, while OCP crystals generated in the presence of a magnetic field exhibited increased length and width of oriented growth. This study provides valuable insights into the influence of mineralization factors in bioprocessing-inspired manufacturing processes.

**Keywords:** octacalcium phosphate; magnetic field; mineralization

## 1. Introduction

Human bone, as an organic/inorganic composite of collagen and apatite crystals, inspires exploration into calcium phosphate/polymer composites as potential candidates for bone tissue scaffolds [1]. Those composites, formed by synthesizing and hybridizing calcium phosphate with polymers, exhibit altered biocompatibility due to their similarity to the inorganic component of natural bone (apatite), high bone conductivity, and high affinity for proteins [2,3].

Bone possesses anisotropic properties, exhibiting weaknesses in tension and shear yet resilience in the longitudinal direction. The alignment of elastic collagen fibers along the bone's stress direction promotes mechanical flexibility. Incorporating calcium phosphate particles into polymers aims to mimic the human bone structure; however, only a few reported calcium phosphate/polymer composites have demonstrated sufficient mechanical strength for bone tissue scaffolds. To achieve anisotropic mechanical properties, controlled dispersion and alignment of calcium phosphate particles with specific size and morphology in the polymer are essential [4]. Particle size and shape also impact biological responses such as cell adhesion and bone regeneration. For instance, variations in hydroxyapatite particle size and morphology in hydroxyapatite/polyethylene composites affect mechanical properties, with larger hydroxyapatite particles decreasing strength and modulus but increasing ductility [5,6]. The two-dimensional morphology of calcium phosphate particles, such as a belt or plate shape, is expected to enhance particles unidirectionally due to a larger surface area with stronger adsorption properties.

Octacalcium phosphate ( $\text{Ca}_8(\text{HPO}_4)_2(\text{PO}_4)_4 \cdot 5\text{H}_2\text{O}$ , hereafter abbreviated as OCP) shares structural similarity with hydroxyapatite ( $\text{Ca}_3(\text{OH})_2(\text{PO}_4)_6$ , henceforth referred to as HA) and is reported to facilitate mineralized tissue formation as an initial precursor phase of HA [7–9]. OCP, under normal physiological conditions, is thermodynamically metastable with respect to HA, and it has been demonstrated that *in vivo* transformation of OCP to HA through hydrolysis takes place [10,11]. This conversion of OCP to HA has facilitated the study of OCP-based composites as bone scaffolds. Two-dimensional OCP particles having



**Citation:** He, W.; Xue, B.; Qian, Q.; Chen, S.; Fu, Z.; Wang, K. Mineralization of Octacalcium Phosphate under Magnetic Field. *Crystals* **2024**, *14*, 463. <https://doi.org/10.3390/cryst14050463>

Academic Editor: Raphaël P. Hermann

Received: 10 April 2024

Revised: 9 May 2024

Accepted: 13 May 2024

Published: 16 May 2024



**Copyright:** © 2024 by the authors. Licensee MDPI, Basel, Switzerland. This article is an open access article distributed under the terms and conditions of the Creative Commons Attribution (CC BY) license (<https://creativecommons.org/licenses/by/4.0/>).

a range of 3–5  $\mu\text{m}$  have been explored for various applications, including adsorption and as capacitors. The size and shape of OCP play important roles in some uses [12]. The 3D flower-like OCP with a size of 2–5  $\mu\text{m}$  was demonstrated to be an efficient  $\text{Pb}^{2+}$  adsorbent. The size of OCP within the polymer hybrids was reported to exert an influence on the capability of bone regeneration and the rate of resorption of the hybrid material [13,14]. Resorption of OCP/collagen by osteoblast-like cells showed enhancement of the composite composing belt-shaped OCP particles with dimensions of 0.5–3  $\mu\text{m}$  compared to those measuring 53–300  $\mu\text{m}$  and pure collagen [15].

Though over two decades of research have advanced our understanding of biomineralization mechanisms and biomimetic mineralization, a significant gap exists in fully achieving a biomimetic transition from structure to function. This discrepancy may be attributed to the following: inadequate simulation of the physiological activity factors of biomineralization [16]. The authentic biomineralization procedure unfolds with cellular participation; thus, biomimetic mineralization necessitates consideration of the impact of physiological activities in conjunction with the aforementioned organic and inorganic milieus for sufficient simulation of the intricate environmental factors of biomineralization [17,18]. The actual biomineralization occurs in a complex environment, apart from organic substrates, inorganic ions, pH value, temperature, and other prevalent direct factors; there are complex electromagnetic fields, gravity fields, and other environmental elements that are frequently overlooked. The effects of these minor environmental factors should not be ignored during the protracted biomineralization process, spanning years [19–21]. Comprehensive simulation of the above factors is an immense task and complicated procedure. The simulation of single factors, from superficial to profound levels, is the logical scientific approach to address the issue.

In our work, the role of magnetic fields in the mineralization of OCP crystals was investigated. The growth of OCP nanocrystals was fulfilled *in vitro* with and without a magnetic field. Different stages of the growth process of OCP nanocrystals during the mineralization were captured; meanwhile, the microstructure of OCP nanocrystals at different positions in the mineralization solutions and gels were demonstrated. Then, the effect of mineralization temperature was studied. The directional growth of OCP crystals with varied conditions depends on the concentration of calcium ions, the mineralization temperature, and the magnetic field.

## 2. Materials and Methods

High-purity materials, including calcium nitrate tetrahydrate ( $\text{Ca}(\text{NO}_3)_2 \cdot 4\text{H}_2\text{O}$ , Merck, Rahway, NJ, USA), sodium phosphate dibasic ( $\text{Na}_2\text{HPO}_4$ , Fisher Scientific, Hampton, NH, USA), and sodium metasilicate nonahydrate ( $\text{Na}_2\text{SiO}_3 \cdot 9\text{H}_2\text{O}$ , Fisher Scientific), with purity exceeding 98%, were utilized in this experiment. All experiments were conducted using triple-distilled water.

A solution of sodium metasilicate nonahydrate with a specific gravity of 1.03 g/cc was mixed with 0.3 M sodium phosphate dibasic solution in a 1:1 ratio. The pH value of the solution was adjusted to 7 through treatment with acetic acid. Subsequently, 5 mL of the above solution was solidified in a centrifuge tube for 1 day to obtain silica gel.

A total of 5 mL of 0.5 M calcium nitrate tetrahydrate solution was added as a supernatant to the gel medium for diffusion. The above samples were mineralized at 37 °C for different periods of time (1, 3, and 5 days). The same samples were mineralized at 50 °C for additional mineralization periods (2, 4, and 8 h). The experiment was repeated with the presence of a magnetic field achieved by placing centrifuge tubes between  $\text{Nd}_2\text{Fe}_{14}\text{B}$  bar magnets spaced approximately 1.5 cm apart, producing a field strength of about 0.3 T as measured with a Gauss meter. The obtained crystals were washed with deionized water, freeze-dried, and subjected to further characterization. Photographs depicting the gel medium after the mineralization process with and without the magnetic field are shown in Figure 1. Liesegang rings (LRs) were classified into Upper LRs, Middle LRs, and Lower LRs, with the crystallization influenced by factors such as temperature, pH, and concentration.

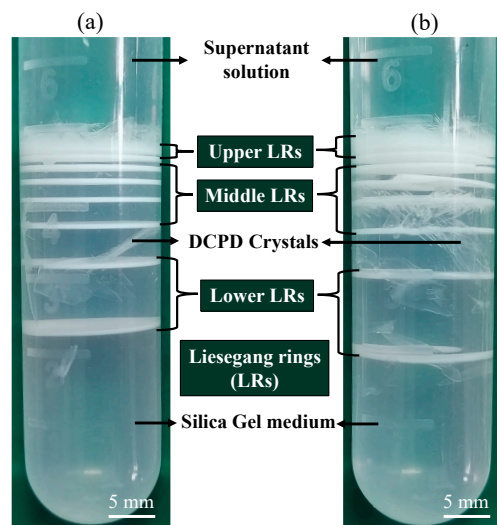


**Figure 1.** Photograph of Liesegang rings and DCPD crystallized in the gel medium (a) without a magnetic field and (b) with a magnetic field.

The X-ray diffraction (XRD) analysis was carried out using an X-ray diffractometer (D8 Advance). Fourier transform infrared spectra (FTIR) were recorded with a Jasco Nexus FTIR spectrometer. Scanning electron microscopy (SEM) micrography and energy-dispersive X-ray (EDX) analysis were carried out using a JSM-7500F SEM. Transmission Electron Microscopy (TEM) images were obtained with a Talos F200S operated at 200 kV.

### 3. Results and Discussion

#### 3.1. Physical Phase Analysis of Crystals in Gel Media

According to the XRD patterns in Figure 2, the main crystalline phase of the Lower LR samples with and without a magnetic field was octacalcium phosphate (OCP) (JCPDS (26-1056)). The (020) peak corresponding to dicalcium phosphate dihydrate only appeared in Lower LR samples mineralized at 37 °C for 5 days. Also, the principal crystalline phase of the DCPD crystals generated in the gel medium was confirmed to be dicalcium phosphate dihydrate (JCPDS card: no 72-0713) (Figure S1). The coexistence of DCPD crystals and Lower LRs may be attributed to the overlapping growth of DCPD crystals and Lower LRs with increasing mineralization time. The presence of a magnetic field resulted in only a slight variation in lattice parameters compared to experiments without a magnetic field [22]. This phenomenon is due to the fact that the presence of a magnetic field only leads to morphological changes in trace amounts of OCP crystals on the surface. The effect of the magnetic field on the overall powder XRD results is negligible.

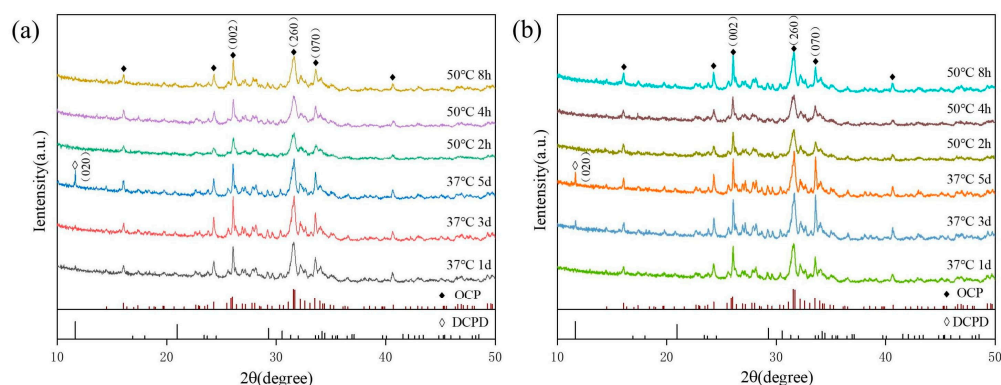


**Figure 2.** XRD patterns of the Lower LR samples (a) without a magnetic field and (b) with a magnetic field.

### 3.2. Effect of External Magnetic Field on the Size and Shape of OCP

The SEM images (Figure S2a–f) of LR samples after mineralization at 25 °C for 14 days revealed the different growth phenomena of OCP crystals without and with magnetic fields. The oriented growth of octacalcium phosphate crystals is observed on the surface of the Middle LRs and Lower LRs in samples under a magnetic field. This indicates that the magnetic field favors the directional growth of octacalcium phosphate crystals. In the sample mineralized under a magnetic field, the average thickness of the directional growth layer increased from 26 µm in Middle LRs to 61 µm in Lower LRs, confirming that increased distance from the gel–supernatant interface is more conducive to the growth of the octacalcium phosphate crystal-oriented layer. The physical phase of the LR sample was determined to be OCP crystals by XRD combined with FTIR spectroscopy analysis (Figure S2g,h).

The mineralization temperature was increased from 25 °C to 37 °C to reduce the mineralization time. Figure 3a–c,a'–c' indicates that OCP crystals in Upper LRs have similar microstructures with and without a magnetic field. However, in the Middle LRs and Lower LRs, the directional growth of OCP crystals could also be observed in samples without a magnetic field (Figure 3f,h,i). In the Middle LRs mineralized for 1 day at 37 °C, the length of the directional layer band crystals increased from 3.6 µm in samples without a magnetic field to 8.5 µm in samples with a magnetic field. In Lower LRs, the length and width of directional layer ribbon crystals were increased from 7.1 µm to 30 µm and from 0.4 µm to 2.1 µm when a magnetic field was applied. Therefore, the directional growth of OCP crystals is not only caused by the mineralization temperature but also by the magnetic field. Both temperature and magnetic field can accelerate the crystallization and growth of OCP crystals. Comparing the samples mineralized under the same conditions, the OCP directional growth length escalated in Lower LRs, whereas the directional growth of OCP crystals was not observed in Upper LRs. These changes in crystal structure and size indicate that the magnetic field has a significant effect on the nucleation and directional growth of OCP. This phenomenon is accounted for by the elevation in the free energy of the nucleus due to the presence of a magnetic field [22–24]. During nucleation, the magnetic anisotropy of nucleated clusters surpasses that of individual molecules, promoting the alignment of the nucleated clusters and fortifying the organization of the nano-sized crystals in the parent solution in relation to the magnetic field. Additionally, the magnetic field accelerates the diffusion process of ions within the gel medium [23,25,26].

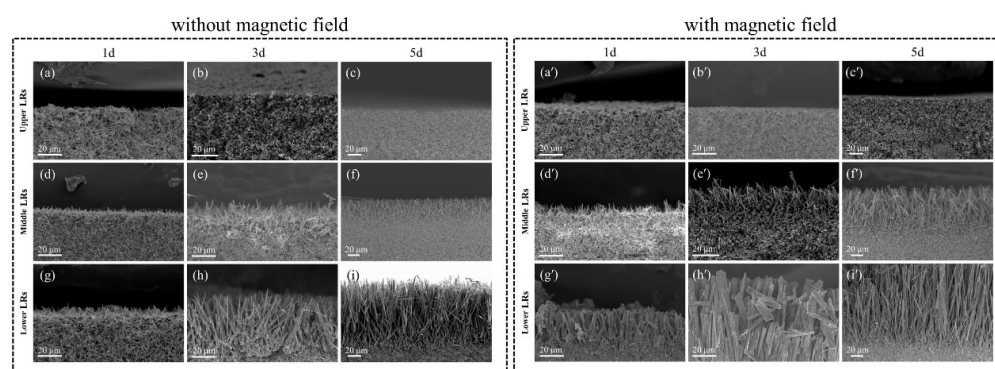


**Figure 3.** SEM micrographs of cross sections of LR samples at 37 °C: (a–c) samples of Upper LRs at 1, 3, and 5 days of mineralization, (d–f) samples of Middle LRs at 1, 3, and 5 days of mineralization, (g–i) samples of Lower LRs at 1, 3, and 5 days of mineralization, (a'–i') control samples under magnetic field.

In addition, the magnetic field also plays a crucial role in the mineralization process. According to the valence bond theory of coordination bonds,  $\text{Ca}^{2+}$  in solution is easy to form  $[\text{Ca}(\text{H}_2\text{O})_6]^{2+}$ , which has a regular octahedral polyhedron and relatively stable structure. When the mineralization solution is applied with a magnetic field, the dipole

moment of water molecules changes to alter the O-H bond length and H-O-H bond angle, which distorts the originally stable  $[\text{Ca}(\text{H}_2\text{O})_6]^{2+}$  octahedral configuration and ultimately leads to its stability decline. The decrease of the stability of  $[\text{Ca}(\text{H}_2\text{O})_6]^{2+}$  leads to the increase of  $\text{Ca}^{2+}$  reactivity, which is conducive to the mineralization of OCP crystals.

A large number of plate and dendrite calcium phosphate dihydrate crystals were observed at the interface of the mineralized fluid and the gel. It is speculated that the high ion concentration at the interface of the mineralized liquid and gel is conducive to the growth of calcium bisphosphate dihydrate crystals but not conducive to the directional growth of OCP crystals.

The orientation and crystal structure of the ribbon particles were further investigated using transmission electron microscopy (TEM). The HRTEM images of the ribbon particles showed a lattice stripe spacing of 0.81 nm and 0.34 nm (Figure S3), corresponding to (010) and (002) crystal planes, confirming the orientation of the ribbon OCP. The striped particles obtained after magnetic field treatment have more diffraction spots and higher crystallinity [27–30].

The mineralization at 50 °C indicates that OCP crystals will develop directionally on the surface of Liesegang rings (Figure 4). There were considerable dissimilarities in the oriented growth crystals of Upper LR, Middle LR, and Lower LR OCP crystals for the 8 h mineralized samples (Figure 4c,f,i), with no oriented growth observed in all Upper LRs. The results further confirm that the OCP directional growth length increases closer to the bottom of the centrifuge tube.

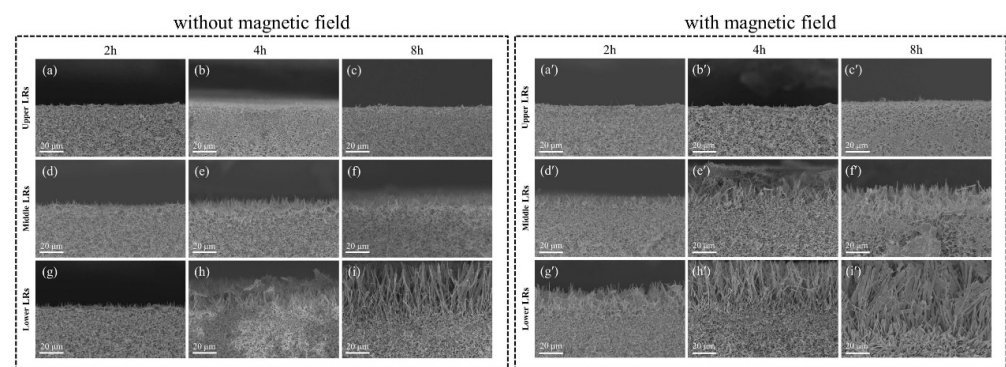


**Figure 4.** SEM micrographs of cross sections of LR samples at 50 °C: (a–c) samples of Upper LRs at 2, 4, and 8 h of mineralization, (d–f) samples of Middle LRs at 2, 4, and 8 h of mineralization, (g–i) samples of Lower LRs at 2, 4, and 8 h of mineralization, (a'–i') control samples under magnetic field.

XRD patterns of the samples mineralized with and without a magnetic field, as seen in Figure 2, show that only OCP crystals were formed at 50 °C; there is no crystal phase of DCPD. This is caused by the increased mineralization temperature, which leads a conversion of unstable calcium bisphosphate dihydrate phases to OCP crystals.

When the mineralization temperature was progressively elevated from 25 °C to 37 °C and then to 50 °C, the time needed for a complete mineralization process decreased. The results also prove that OCP crystals preferred to grow directionally under higher mineralization temperatures, a magnetic field, and a lower calcium ion concentration.

### 3.3. Effect of External Magnetic Field on the Rate of OCP Directional Growth

Based on these SEM images, the growth rates of directional OCP crystals in Lower LRs mineralized at different conditions were calculated and are presented in Table 1. For samples mineralized at 37 °C, the magnetic field slightly accelerates the growth rate of mineralization, which increases from 0.98 to 1.19  $\mu\text{m}/\text{h}$  in length and 0.02 to 0.05  $\mu\text{m}/\text{h}$  in width. For samples mineralized at 50 °C, the magnetic field dramatically accelerates the growth rate of mineralization, which increases from 7.64 to 11.27  $\mu\text{m}/\text{h}$  in length and 0.17 to 0.23  $\mu\text{m}/\text{h}$  in width. The results also prove that the mineralization temperature

promotes the directional growth of OCP crystals. The increase in the growth rate of octacalcium phosphate crystals can be attributed to the accelerating effect of the magnetic field in the ion diffusion phase. The charged ions in the gel will move directionally in the presence of an applied magnetic field, making it easier for reactions between anions and cations [22,24]. This contributes to the nucleation growth process of octacalcium phosphate crystals. In addition, the distortion of complex ions in the gel caused by the magnetic field will increase the supersaturation of  $\text{Ca}^{2+}$ .

**Table 1.** Dimensions of directional OCP crystals in Lower LRs with and without magnetic field at a mineralization temperature of 37 °C and 50 °C, respectively.

Temperature (°C)	Time (hours)	Lengths of Directional OCP Crystals in Lower LRs (μm)		Widths of Directional OCP Crystals in Lower LRs (μm)	
		Without Magnetic Field	With Magnetic Field	Without Magnetic Field	With Magnetic Field
37	24	7.1	30	0.4	2.1
	72	50	85	1.4	4.7
	120	102	144	1.9	7.2
	Growth rate (μm/hour)	0.98	1.19	0.02	0.05
50	2	3.7	12.7	0.3	0.8
	4	15.2	43.7	0.5	1.2
	8	48.8	82	1.3	2.2
	Growth rate (μm/hour)	7.64	11.27	0.17	0.23

#### 4. Discussion

The directional growth of OCP crystals was successfully controlled via mineralization under different conditions, as confirmed by XRD and SEM. OCP crystal growth was found to be dependent on mineralization temperature, mineralization time, and the magnetic field. Higher temperatures significantly reduced the mineralization time, which is crucial for the directional growth of OCP crystals. OCP crystals generated in the presence of a magnetic field exhibited increased length and width of oriented growth compared to those without a magnetic field. The analysis of the mineralization mechanism of octacalcium phosphate clarifies that the effect of the magnetic field on the mineralization of octacalcium phosphate mainly leads to an increase in the free energy of its nuclei, which enhances the ordering of the crystals with respect to the magnetic field. In the ion diffusion stage, the magnetic field mainly induces the modification of the water molecule bond angles, resulting in the aberration of  $[\text{Ca}(\text{H}_2\text{O})_6]^{2+}$  complex ions. This study provides valuable insights into the influence of mineralization factors, particularly magnetic fields, in bioprocessing-inspired manufacturing processes.

**Supplementary Materials:** The following supporting information can be downloaded at: <https://www.mdpi.com/article/10.3390/cryst14050463/s1>, Figure S1: XRD pattern of DCPD crystals generated in gel medium; Figure S2: SEM images of LRs in samples after mineralization at 25 °C for 14 days (a–c) without magnetic field, (d–f) with magnetic field; (g) XRD and (h) FT-IR of Lower LRs; Figure S3: HRTEM images and corresponding FFT patterns of belt-like particle: (a) Sample of Lower LRs without magnetic field at 37 °C and (b) Sample of Lower LRs with magnetic field at 37 °C.

**Author Contributions:** Funding acquisition, Z.F. and K.W.; investigation, W.H. and B.X.; methodology, W.H., Q.Q. and S.C.; supervision, Z.F. and K.W.; writing—original draft, W.H.; writing—review and editing, K.W. All authors have read and agreed to the published version of the manuscript.

**Funding:** This research was funded by the National Key Research and Development Program of China (2021YFA0715700) and the Open Fund of Hubei Longzhong Laboratory. Dr. Kun Wang

appreciates the support of the State Key Laboratory of Materials Processing and Die & Mould Technology, Huazhong University of Science and Technology.

**Data Availability Statement:** Data is contained within the article or Supplementary Materials.

**Conflicts of Interest:** The authors declare no conflicts of interest.

## References

1. Safronova, T.V.; Putlyaev, V.I.; Filippov, Y.Y.; Vladimirova, S.A.; Zuev, D.M.; Cherkasova, G.S. Synthesis of Calcium-Phosphate Powder from Calcium Formiate and Ammonium Hydrophosphate for Obtaining Biocompatible Resorbable Biphase Ceramic Materials. *Glass Ceram.* **2017**, *74*, 185–190. [[CrossRef](#)]
2. Chocholata, P.; Kulda, V.; Babuska, V. Fabrication of Scaffolds for Bone-Tissue Regeneration. *Materials* **2019**, *12*, 25. [[CrossRef](#)] [[PubMed](#)]
3. Manohar, S.S.; Das, C.; Kakati, V. Bone Tissue Engineering Scaffolds: Materials and Methods. *3D Print. Addit. Manuf.* **2024**, *11*, 347–362. [[CrossRef](#)] [[PubMed](#)]
4. Musskaya, O.N.; Kulak, A.I.; Krut'ko, V.K.; Lesnikovich, Y.A.; Kazbanov, V.V.; Zhitkova, N.S. Preparation of Bioactive Mesoporous Calcium Phosphate Granules. *Inorg. Mater.* **2018**, *54*, 117–124. [[CrossRef](#)]
5. Czikó, M.; Bog, E.S.; Diudea, M.V.; Barabás, R. Research on Hydroxyapatite Based Composite Materials. *Rev. Roum. Chim.* **2014**, *59*, 353–357.
6. Macuvele, D.L.P.; Nones, J.; Matsinhe, J.V.; Lima, M.M.; Soares, C.; Fiori, M.A.; Riella, H.G. Advances in ultra high molecular weight polyethylene/hydroxyapatite composites for biomedical applications: A brief review. *Mater. Sci. Eng. C* **2017**, *76*, 1248–1262. [[CrossRef](#)]
7. Ding, X.X.; Li, A.M.; Yang, F.S.; Sun, K.N.; Sun, X.N.  $\beta$ -tricalcium phosphate and octacalcium phosphate composite bioceramic material for bone tissue engineering. *J. Biomater. Appl.* **2020**, *34*, 1294–1299. [[CrossRef](#)] [[PubMed](#)]
8. Yokoi, T.; Goto, T.; Kato, T.; Takahashi, S.; Nakamura, J.; Sekino, T.; Ohtsuki, C.; Kawashita, M. Hydroxyapatite Formation from Octacalcium Phosphate and Its Related Compounds: A Discussion of the Transformation Mechanism. *Bull. Chem. Soc. Jpn.* **2020**, *93*, 701–707. [[CrossRef](#)]
9. Gemelli, E.; Resende, C.X.; Soares, G.D.D. Nucleation and growth of octacalcium phosphate on treated titanium by immersion in a simplified simulated body fluid. *J. Mater. Sci.-Mater. Med.* **2010**, *21*, 2035–2047. [[CrossRef](#)]
10. Brasil, L.R.; Rodrigues, M.C.; Hewer, T.L.R.; Fronza, B.M.; Arana-Chavez, V.E.; Vichi, F.M.; Madsen, H.E.L.; Braga, R.R. Effect of temperature and reactant concentration on calcium phosphate precipitation. *J. Cryst. Growth* **2020**, *552*, 7. [[CrossRef](#)]
11. Wang, K.F.; Luo, F.X.; Wang, L.; Zhang, B.Q.; Fan, Y.J.; Wang, X.; Xu, D.G.; Zhang, X.D. Biomineralization from the Perspective of Ion Aggregation: Calcium Phosphate Nucleation in the Physiological Environment. *ACS Appl. Mater. Interfaces* **2021**, *13*, 49519–49534. [[CrossRef](#)]
12. Shin, Y.S.; Jo, M.K.; Cho, Y.S.; Yang, S.H. Diffusion-Controlled Crystallization of Calcium Phosphate in a Hydrogel toward a Homogeneous Octacalcium Phosphate/Agarose Composite. *ACS Omega* **2022**, *7*, 1173–1185. [[CrossRef](#)] [[PubMed](#)]
13. Shen, D.H.; Horiuchi, N.; Nozaki, S.; Miyashin, M.; Yamashita, K.; Nagai, A. Synthesis and enhanced bone regeneration of carbonate substituted octacalcium phosphate. *Bio-Med. Mater. Eng.* **2017**, *28*, 9–21. [[CrossRef](#)] [[PubMed](#)]
14. Hamai, R.; Sakai, S.; Shiwaku, Y.; Anada, T.; Tsuchiya, K.; Ishimoto, T.; Nakano, T.; Suzuki, O. Octacalcium phosphate crystals including a higher density dislocation improve its materials osteogenicity. *Appl. Mater. Today* **2022**, *26*, 12. [[CrossRef](#)]
15. Kouketsu, A.; Matsui, K.; Kawai, T.; Ezoe, Y.; Takahashi, T.; Kamakura, S. Teriparatide with Octacalcium Phosphate Collagen Composite Stimulates Osteogenic Factors. *Tissue Eng. Part A* **2022**, *28*, 125–135. [[CrossRef](#)]
16. Sovljanski, O.; Pezo, L.; Grahovac, J.; Tomic, A.; Ranitovic, A.; Cvetkovic, D.; Markov, S. Best-performing Bacillus strains for microbiologically induced  $\text{CaCO}_3$  precipitation: Screening of relative influence of operational and environmental factors. *J. Biotechnol.* **2022**, *350*, 31–41. [[CrossRef](#)]
17. Li, Z.C.; Zeng, Y.H.; Ren, Q.; Ding, L.J.; Han, S.L.; Hu, D.; Lu, Z.Q.; Wang, L.Y.; Zhang, Y.M.; Zhang, L.L. Mineralization promotion and protection effect of carboxymethyl chitosan biomodification in biomimetic mineralization. *Int. J. Biol. Macromol.* **2023**, *234*, 12. [[CrossRef](#)]
18. Zhang, X.L.; Fan, Z.H.; Lu, Q.; Huang, Y.L.; Kaplan, D.L.; Zhu, H.S. Hierarchical biomineralization of calcium carbonate regulated by silk microspheres. *Acta Biomater.* **2013**, *9*, 6974–6980. [[CrossRef](#)]
19. Grenier, C.; Román, R.; Duarte, C.; Navarr, J.M.; Rodriguez-Navarro, A.B.; Ramajo, L. The combined effects of salinity and pH on shell biomineralization of the edible mussel *Mytilus chilensis*. *Environ. Pollut.* **2020**, *263*, 10. [[CrossRef](#)]
20. Tanasa, E.; Zaharia, C.; Hudita, A.; Radu, I.C.; Costache, M.; Galateanu, B. Impact of the magnetic field on 3T3-E1 preosteoblasts inside SMART silk fibroin-based scaffolds decorated with magnetic nanoparticles. *Mater. Sci. Eng. C* **2020**, *110*, 13. [[CrossRef](#)] [[PubMed](#)]
21. Ortiz, F.; Díaz-Barríos, A.; Lopez-Cabaña, Z.E.; González, G. Effect of the Electric Field on the Biomineralization of Collagen. *Polymers* **2023**, *15*, 19. [[CrossRef](#)] [[PubMed](#)]
22. Baskar, S.; Ramya, J.R.; Arul, K.T.; Nivethaa, E.A.K.; Pillai, V.P.M.; Kalkura, S.N. Impact of magnetic field on the mineralization of iron doped calcium phosphates. *Mater. Chem. Phys.* **2018**, *218*, 166–171. [[CrossRef](#)]

23. Sundaram, N.M.; Girija, E.K.; Ashok, M.; Anee, T.K.; Vani, R.; Suganthi, R.V.; Yokogawa, Y.; Kalkura, S.N. Crystallisation of hydroxyapatite nanocrystals under magnetic field. *Mater. Lett.* **2006**, *60*, 761–765. [[CrossRef](#)]
24. Yanovska, A.; Kuznetsov, V.; Stanislavov, A.; Danilchenko, S.; Sukhodub, L. A study of brushite crystallization from calcium-phosphate solution in the presence of magnesium under the action of a low magnetic field. *Mater. Sci. Eng. C* **2012**, *32*, 1883–1887. [[CrossRef](#)] [[PubMed](#)]
25. Kuznetsov, V.N.; Yanovska, A.A.; Stanislavov, A.S.; Danilchenko, S.N.; Kalinkevich, A.N.; Sukhodub, L.F. Controllability of brushite structural parameters using an applied magnetic field. *Mater. Sci. Eng. C* **2016**, *60*, 547–553. [[CrossRef](#)] [[PubMed](#)]
26. Tripathi, G.; Miyazaki, T. Spontaneous fabrication of octacalcium phosphate: Synthesis conditions and basic characterizations. *Bull. Mat. Sci.* **2021**, *44*, 6. [[CrossRef](#)]
27. Iijima, M.; Onuma, K. Particle-size-dependent octacalcium phosphate overgrowth on  $\beta$ -tricalcium phosphate substrate in calcium phosphate solution. *Ceram. Int.* **2018**, *44*, 2146–2157. [[CrossRef](#)]
28. Petrakova, N.V.; Teterina, A.Y.; Mikheeva, P.V.; Akhmedova, S.A.; Kuvshinova, E.A.; Sviridova, I.K.; Sergeeva, N.S.; Smirnov, I.V.; Fedotov, A.Y.; Kargin, Y.F.; et al. In Vitro Study of Octacalcium Phosphate Behavior in Different Model Solutions. *ACS Omega* **2021**, *6*, 7487–7498. [[CrossRef](#)] [[PubMed](#)]
29. Saengdet, P.; Ogawa, M. Directional growth of octacalcium phosphate using micro-flow reactor mixing and subsequent aging. *RSC Adv.* **2021**, *11*, 15969–15976. [[CrossRef](#)]
30. McDonogh, D.P.; Kirupananthan, P.; Gebauer, D. Counterintuitive Crystallization: Rate Effects in Calcium Phosphate Nucleation at Near-Physiological pH. *Cryst. Growth Des.* **2023**, *23*, 7037–7043. [[CrossRef](#)]

**Disclaimer/Publisher’s Note:** The statements, opinions and data contained in all publications are solely those of the individual author(s) and contributor(s) and not of MDPI and/or the editor(s). MDPI and/or the editor(s) disclaim responsibility for any injury to people or property resulting from any ideas, methods, instructions or products referred to in the content.